67º congresso 2012 abm
67th abm international congress
ISSN 1516-392X

A DISLOCATION DENSITY-BASED ANALYSIS OF A COMMERCIAL COPPER DEFORMED VIA ECAE TECHNIQUE[1]

Neil de Mederos[2]
Luciano Pessanha Moreira[2]

Abstract
In this work, finite-element models and upper-bound solutions are proposed to analyze the processing of a commercial copper via equal channel angular extrusion technique (ECAE). In this way, a dislocation density constitutive formulation is adopted to account for the work-hardening and recovery phenomena which take place in this process. In relation to numerical modeling, the three-dimensional general integration procedure based upon the elastic-predictor and plastic-corrector algorithm is firstly presented within the context of the plastic flow theory along with isotropic work-hardening. Then, the implemented dislocation density model is validated for both implicit and explicit finite element integration techniques *vis-à-vis* to the experimental uniaxial tensile data reported in the literature for single ECAE pass of a commercial copper. Otherwise, by using the upper-bound method, the extrusion force is calculated regarding the effects of friction, tooling geometry and also material mechanical behavior with effective stress measure provided by dislocation density constitutive model. The introduction of backpressure effect showed consistent increasing of extrusion force, effective plastic strain and density dislocation in comparison with the predictions that neglected this parameter. Finally, the proposed upper-bound solutions could be validated in terms of processing load, effective plastic strain and density dislocation by equivalent obtained numerical predictions.
Key words: ECAE; Finite element; Upper-bound method; Density dislocation.

[1] *Technical contribution to 67th ABM International Congress, July, 31th to August 3rd, 2012, Rio de Janeiro, RJ, Brazil.*
[2] *D.Sc., Professor, Program of Post graduation in Metallurgical Engineering, Federal Fluminense University (UFF), RJ, Brasil; neil@metal.eeimvr.uff.br; luciano.moreira@metal.eeimvr.uff.br.*

ISSN 1516-392X

1 INTRODUCTION

The equal channel angular extrusion (ECAE) is a severe plastic deformation process employed to produce bulk ultra-fine grained materials with improved mechanical properties[1,2]. In the ECAE process, a well lubricated billet is forced to pass through a two-channel die with constant cross-sectional area. The workpiece undergoes a large amount of plastic strain by simple shear within the deformation zone located at the channels die intersection[3]. Thus, the knowledge of the kinematics of deformation is essential to understand the basic mechanisms controlling the grain refinement in the ECAE processing. Semiatin el al.[4] reviewed the models proposed in the literature to describe the mechanics and the deformation pattern resulting from the ECAE process. Some analytical and numerical modeling approaches are recalled hereafter. Firstly, the macroscopic deformation models based upon classical metal forming analytical solutions such as the slip-line field and upper-bound theorem[5-8]. Secondly, the flow models wherein the actual strain history during the ECAE process is derived from the descriptions of the kinematics of deformation. In this framework, the crystallographic texture and microstructural evolution associated with the deformation histories resulting from different ECAE routes can be directly evaluated via polycrystalline plasticity approaches, as in Gholinia et al.[9], Beyerlein et al.[10] and Tóth et al.[11]. Lastly, the continuum models based upon the finite element method which has been broadly adopted to analyze the effects of relevant parameters such as geometrical, tribological and rheological as well as processing conditions on the billet stress-strain distributions, extrusion force, temperature changes, grain refinement and mechanical properties[12-15]. Into this context, upper-bound and finite element density dislocation-based models are proposed to investigate the influence of rhelology and processing conditions during the single pass deformation of a commercial copper by means of equal channel angular extrusion technique.

2 METHODS

2.1 Constitutive Equations

Firstly, the total strain-rate tensor is described by the additive decomposition assuming the small deformation theory as:

$$\dot{\varepsilon} = \dot{\varepsilon}^{e} + \dot{\varepsilon}^{p} \quad (1)$$

In Equation 1 the elastic part e is described by the linear isotropic elasticity Hooke's law defined as:

$$\dot{\varepsilon}^{e} = S^{e} : \dot{\sigma} \quad (2)$$

Where $\mathbf{S^e}$ is the elastic compliances forth order tensor and $\dot{\sigma}$ is the Cauchy stress-rate tensor. The plastic part *p* is defined assuming the associated plastic flow rule where the plastic potential is identified by the yield function as:

$$\dot{\varepsilon}^{p} = \dot{\bar{\varepsilon}} \frac{\partial f}{\partial \sigma} \quad (3)$$

In Equation 3 $\dot{\bar{\varepsilon}}$ is the effective plastic strain-rate and f is the yield function defined under the isotropic work-hardening assumption as:

$$f(\sigma, \bar{\varepsilon}, \dot{\bar{\varepsilon}}) = F(\sigma) - \bar{\sigma}(\bar{\varepsilon}, \dot{\bar{\varepsilon}}) \quad (4)$$

Where **F(σ)** is a first degree homogeneous stress function which describes the yield locus and $\bar{\sigma}$ is an effective stress measure which, in turn, may depend of either the accumulated plastic strain or strain-rate effective quantities. In order to describe the

ISSN 1516-392X

experimental yield loci of quasi-isotropic BCC and FCC metals the Drucker's isotropic yield criterion is adopted. This criterion is defined as a function of the second J_2 and third J_3 invariants of the deviatory stress tensor and a material parameter c as:

$$F(\sigma) = (3J_2)^{1/2}\left[1 - c\left(\frac{J_3^2}{J_2^3}\right)\right]^{1/6} \quad (5)$$

The recommended c-values to fit polycrystalline yield loci for isotropic BCC and FCC isotropic metals are equal to 1.35 and 2.025 (used here), respectively [16].
The effective stress measure is described by a Voce type law as:

$$\bar{\sigma} = \bar{\sigma}_s + (\bar{\sigma}_0 - \bar{\sigma}_s)\ \exp\left[\frac{-(\bar{\varepsilon} - \bar{\varepsilon}_0)}{\bar{\varepsilon}_r}\right] \quad (6)$$

Where $\bar{\varepsilon}_0$ and $\bar{\sigma}_0$ are the strain and stress measures corresponding to the yield stress whereas $\bar{\sigma}_s$ is flow-stress saturation that corresponds to strain relaxation $\bar{\varepsilon}_r$.
The strain relaxation is calculated by:

$$\bar{\varepsilon}_r = \frac{2\,\bar{\sigma}_s}{MGbk_1\alpha}\left(\frac{\dot{\bar{\varepsilon}}}{\dot{\hat{\varepsilon}}}\right)^{-1/m} \quad (7)$$

Where in M, G, b, k_1, α and m denote Taylor factor, shear modulus, Burger's vector, material parameter associated to dislocation storage, material constant and the strain-rate sensitivity exponent, respectively. Also, the flow-stress saturation is given by:

$$\bar{\sigma}_s = \hat{\sigma}_{so}\left(\frac{\dot{\bar{\varepsilon}}}{\dot{\varepsilon}_o}\right)^{\frac{1}{n+m}} \quad (8)$$

Where $\hat{\sigma}_{so}$ is the saturation stress at the reference condition $\dot{\varepsilon}_o$.
In this work, the Kocks [17] of is used to estimate a multiscale relationship between the effective measures of stress and strain, that is,

$$\bar{\sigma} = \hat{\sigma}\left(\frac{\dot{\bar{\varepsilon}}}{\dot{\hat{\varepsilon}}}\right)^{1/m} \quad (9)$$

According to Taylor hardening theory, the mesoscopic yield stress, $\hat{\sigma}$, can be related with a given dislocation density, ρ, by:

$$\hat{\sigma} = M\alpha Gb\sqrt{\rho} \quad (10)$$

And a viscoplastic rule to the mesoscopic saturation stress, $\hat{\sigma}_s$ [17]:

$$\hat{\sigma}_s = \hat{\sigma}_{so}\left(\frac{\dot{\bar{\varepsilon}}}{\dot{\varepsilon}_0}\right)^{1/n} \quad (11)$$

Where n is the work-hardening exponent.
The macroscopic effective stress defined in Equation 6 is here estimated by using the Kocks-Mecking [18] dislocation density model. Thus, the differential evolution of dislocation density, ρ, associated to the effective plastic strain $\bar{\varepsilon}$ is given by:

$$\frac{d\rho}{d\bar{\varepsilon}} = M\left[k_1\rho^{1/2} - k_2\rho\right] \quad (12)$$

where k_2 is related to dynamic recovering phenomenon. Also, the Taylor factor although be highly depends of deformation path, it is fixed in the present work. Equation 12 can be written in an incremental form to be solved as,

ISSN 1516-392X

$$\Delta\rho = M\left[k_1\rho_0^{1/2} - k_2\rho_0\right]\Delta\bar{\varepsilon} \quad (13)$$

Where ρ_0 denotes the initial dislocation density. And

$$\rho_f = \rho_o + \Delta\rho \quad (14)$$

Where ρ_f defines the final dislocation density attributed to the workpiece after a single pass of ECAE. The values assumed for M, k_1, k_2 and ρ_0 were experimentally obtained to pure copper by Dalla Torre et al. [19] and they are listed in Table 1.

Table 1. Parameters estimated to pure copper processed by ECAE[19]

k_1 (mm^{-1})	k_2	α	b (mm)	ρ_0 (mm^{-2})	M	m	$\dot{\bar{\varepsilon}}_o$ (s^{-1})
$8{,}32 \times 10^7$	4,777	0,33	$2{,}56 \times 10^{-7}$	$2{,}90 \times 10^7$	3,06	500	1

Assuming the hypothesis of accumulated effective plastic strain, it is clear that $\bar{\varepsilon}$ varies from zero to the final value attained after the processing, that is, $\Delta\bar{\varepsilon} = \bar{\varepsilon}$. Thus, Equation 13 can be rewritten as,

$$\Delta\rho = M\left[k_1\rho_0^{1/2} - k_2\rho_0\right]\bar{\varepsilon} \quad (15)$$

The elastic-plastic behavior is then completed by introducing the evolution of the effective stress which can be given in a rate form by:

$$\dot{\bar{\sigma}} = H(\bar{\sigma})\,\dot{\bar{\varepsilon}} \quad (16)$$

2.2 ECAE Analytical Modeling

The upper bound method is based on the virtual works principle providing a maximum value to the work rate dissipated on a certain surface. In plasticity problems, for instance, in metal forming analysis, this upper limit is achieved by considering a kinematically admissible velocity field that satisfies both incompressibility and velocity boundary conditions. Thus, the energy portion dissipated by the external forces is equated to that resulting from the plastic deformation process. According to Kobayashi et al. [20], the upper bound method is defined as:

$$\int_V \sigma_{ij}^{*}\dot{\varepsilon}_{ij}^{*}dV + \int_{S_D} \kappa\left|\Delta v^{*}\right|dS - \int_{S_F} F_i v_i^{*}dS \geq \int_{S_u} F_i v_i dS \quad (17)$$

Where the first term denotes the power dissipated due to realized plastic work during the material processing, the second portion represents the energy dissipated along the discontinuity velocity surfaces and the third term is associated to power dissipated by external forces imposed on the material.

Pérez and Luri [21], using the upper-bound method, and adopting the hypothesis of constant pressing velocity, V_0, proposed solutions for estimating the pressing force, P, for perfectly plastic materials and introducing the effects of tooling geometry. However, the effect of external prescribed forces, also called as backpressure, which must be introduced in the third term of Equation 17, was not considered by these authors. Thus,

$$P = WL\kappa\left\{\frac{(\pi-\Phi)}{\sin\left(\frac{\Phi\pm\beta}{2}\right)} + f\left[\frac{2H}{L} + (\pi-\Phi)\left(\frac{R_{inner}+R_{outer}}{L}\right)\left(1-\frac{1}{\sin\left(\frac{\Phi\pm\beta}{2}\right)}\right) + \frac{2H}{W}\right]\right\} \quad (18)$$

ISSN 1516-392X

Where κ, Φ, f, H, L e W denote the pure shear yield stress, die channels intersection angle, friction factor and sample geometrical parameters, respectively. Also, R_{inner} and R_{outer} denote the inner and outer tooling fillet radii.
The angle β related to the die geometries showed in Fig. 1 is calculated by [21],

$$\beta = 2\arctan\left\{\frac{(R_{outer}-R_{inner})\tan[\Phi/2]}{L+(R_{inner}-R_{outer})+L\tan^2[\Phi/2]}\right\} \rightarrow R_{inner} < R_{outer}$$

$$\beta = 2\arctan\left\{\frac{(R_{inner}-R_{outer})\tan[\Phi/2]}{L+(R_{inner}-R_{outer})+L\tan^2[\Phi/2]}\right\} \rightarrow R_{inner} > R_{outer} \quad (19)$$

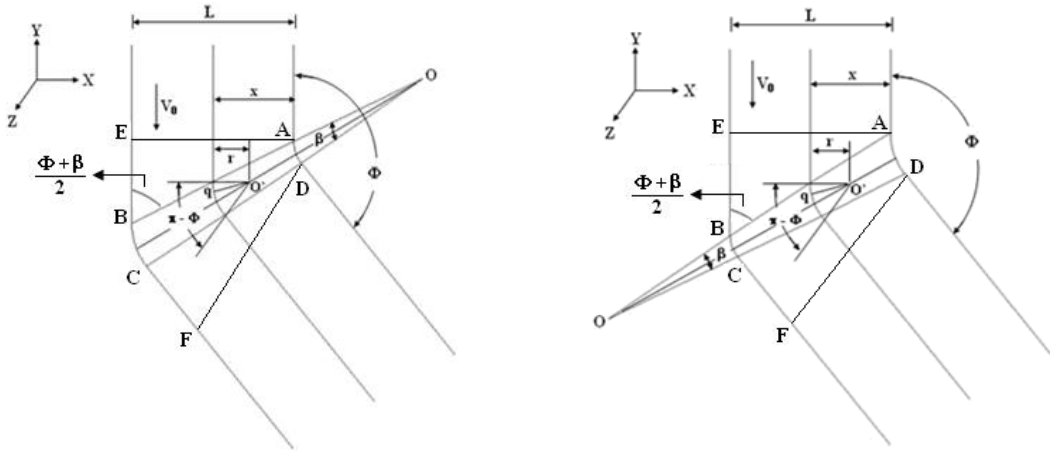

(a) (b)

Figure 1. Die geometries considered in the upper-bound modeling [22]. (a) R_{inner} < outer, R_{outer}, and (b) R_{inner} > R_{outer}.

For an in-plane pure shear (S_{12} = S_{21} = κ other S_{ij} = 0) we have [22],

$$\kappa = \left\{\frac{1}{\sqrt{3}}\left[1-\left(\frac{4c}{27}\right)\right]^{1/6}\right\}\bar{\sigma} \quad (20)$$

Adopting the solutions proposed by Luri et al [23] to the calculation of the shear plastic strain and according to Medeiros et al. [22]:

$$\bar{\varepsilon} = \frac{1}{\sqrt{3}}\left\{2\cot g\left(\frac{\Phi\pm\beta}{2}\right)+(\pi-\Phi)\left[1-\cot g\left(\frac{\Phi\pm\beta}{2}\right)tg\left(\frac{\Phi}{2}\right)\right]\right\} \quad (21)$$

The deformation time used to predict the effective plastic strain rate in Eq. (6) when the material crosses the die geometries presented in Fig. 1, is calculated by [22]:

$$t = \frac{L}{V_0}\left\{2\cot g\left(\frac{\Phi\pm\beta}{2}\right)+\frac{(\pi-\Phi)}{L}\left(1-\cot g\left(\frac{\Phi+\beta}{2}\right)tg\left(\frac{\Phi}{2}\right)\right)\left[R_{int}+L\left(1-\cot g\left(\frac{\Phi\pm\beta}{2}\right)tg\left(\frac{\Phi}{2}\right)\right)\right]\right\} \quad (22)$$

Where V_0 defines the pressing velocity.
The extrusion force was calculated for two distinct cases. Firstly, neglecting backpressure effect by using Equation 18 with the yield shear stress κ calculated with the presented dislocation density formulation by Equations 6 and 20. Then, the backpressure, named as p_{BP}, was introduced in the third term of Equation 23 and the pressing force was predicted by:

ISSN 1516-392X

$$P = WL\left\{\kappa\left\{\frac{(\pi-\Phi)}{\sin\left(\frac{\Phi\pm\beta}{2}\right)}+f\left[\frac{2H}{L}+(\pi-\Phi)\left(\frac{R_{inner}+R_{outer}}{L}\right)\left(1-\frac{1}{\sin\left(\frac{\Phi\pm\beta}{2}\right)}\right)+\frac{2H}{W}\right]\right\}+p_{BP}\right\} \quad (23)$$

It is important to note that the backpressure force increases the pressing force due its additive contribution in Equation 23. In fact, the parameter p_{BP} is contrary to the passage of the billet towards die exit channel, as shown later in Figure 2.
In the analytical evaluations, it was considered a billet with 20 mm of width and 80 mm length. Also, the tooling channels were intersected at Φ = 90º and without fillet radii. Also, for purposes of comparison, the predictions of extrusion force, effective plastic strain and density dislocation were obtained for the cases without and with the imposition of a backpressure of 25 MPa, according to the experiments performed by Dalla Torre et al. [19] with pure cooper. On the other hand, a friction factor of 0.14 was attributed along the workpiece-tooling interfaces to reproduce an ideal lubrication condition according to Drucker's plasticity criterion. In all analyzed cases, the extrusion velocity of 2 mm/s was assumed.

2.3 ECAE Numerical Modeling

2.3.1 General integration method

The Abaqus finite element commercial code provides at the beginning of the time step, for each element integration point, the stress tensor components, σ_{ij}, the increments of the total strain tensor, $\Delta\varepsilon_{ij}$, and all the internal or user defined state variables. Bearing in mind deformation-driven problems, as in displacement based and mixed finite element formulations, the stress state at the end of the time step in then obtained from the strain history by means of an integration of the rate constitutive equations. The general integration procedure is based upon the elastic predictor-plastic corrector commonly known as the return mapping algorithm. In order to abridge the notation, let us denote ξ^t as the current value of all variables at the beginning of the time step, ξ^{Trial} as the quantities referring to the elastic prediction and $\xi^{t+\Delta t}$ as the corrected values determined at the end of the time step.
Firstly, the trial stress components are computed from an elastic prediction using the generalized Hooke's law together with the total strain increments, namely,

$$\sigma_{ij}^{Trial} = \sigma_{ij}^{t} + C_{ijkl}^{e}\Delta\varepsilon_{kl} \quad (24)$$

Where C_{ijkl}^{e} is the 4th order linear isotropic elasticity tensor defined as a function of the Lamè's coefficients as:

$$C_{ijkl}^{e} = \lambda\,\delta_{ij}\,\delta_{kl} + \mu(\delta_{ik}\,\delta_{jl} + \delta_{il}\,\delta_{jk}) \quad (25)$$

The elastic-plastic loading may occur during the current time step if the yield condition given by Equation 4 is violated by the trial state of stress, that is,

$$F(\sigma_{ij}^{Trial}) - \overline{\sigma}(\overline{\varepsilon}^{t}, \dot{\overline{\varepsilon}}^{t}) \geq 0 \quad (26)$$

Then, the new state of stress is obtained from the plastic correction of the trial state according to the implicit and explicit integration techniques available in the ABAQUS FE code. The integration procedure is detailed elsewhere [24]

2.4 ECAE FE Modeling

In this work, is considered the experimental results obtained by Dalla Torre et al. [19] for a commercial copper processed via ECAE with route BC. Two distinct cases is

ISSN 1516-392X

simulated, that is, the first neglecting the effect of backpressure and the second with a back-pressure of 25 MPa. In both cases a plunger speed of 2 mm/s is employed. The workpiece has a square cross-section of 20 mm wide and 80 mm length. Since the main deformation mode of the ECAE process is simple shear and the workpiece cross-section remains unchanged, a plane-strain finite element model is proposed to reduce the computational time. The tooling is described by analytical rigid surfaces whereas the workpiece is modeled by 5,000 plane-strain CPE4R solid elements with reduced integration, as depicted in Figure 2. Also, the friction between the tooling and workpiece is described by the Coulomb's law with μ = 0.08. The numerical simulations were performed with the ABAQUS 6.9 with implicit temporal integration as a quasi-static analysis.

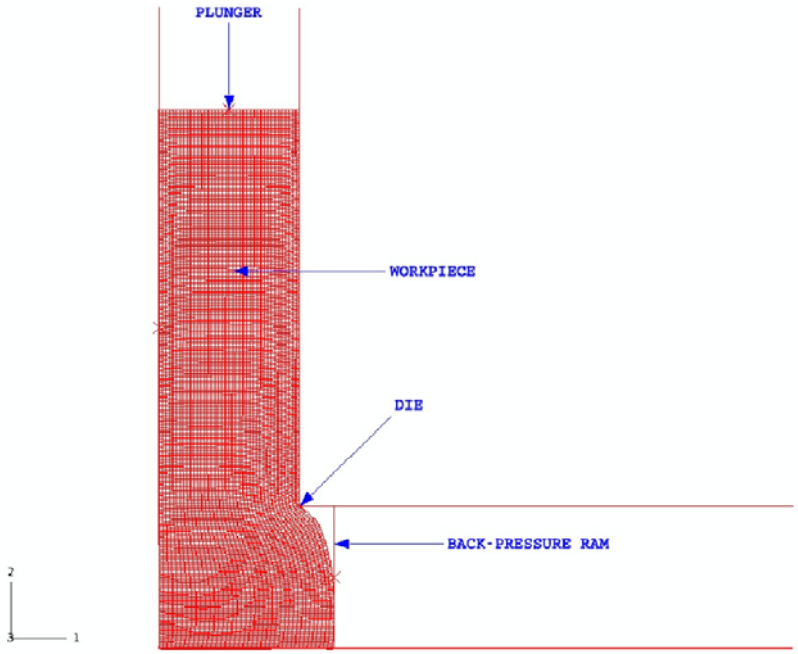

Figure 2. ECAE plane strain finite element model.

3 RESULTS AND DISCUSSION

Figure 3 presents the results of extrusion force obtained with the proposed finite element models during the processing of pure cooper by single-pass of ECAE. One can observe that the curves display similar tendencies, that is, an abrupt increasing of load after ~ 7 mm of punch displacement until their maximum values, characterized by static friction [25] and then it was noted a decreasing of the force until 15 mm followed by successive oscillations. These oscillations are related to continuous plastic deformation imposed on the workpiece when it crosses the die channels intersection region. However, by comparing both load diagrams, it is clear that when the backpressure is introduced into the ECAE tooling, the needed processing force increased to 166 kN after 7 mm of displacement, see the green solid curve, while without backpressure and for the same punch movement the maximum load prediction obtained was ~ 164 kN. It is important to explain that the small influence provided to the backpressure on the extrusion force is due to low processing velocity of 2 mm/s, i.e., we have a quasi static simulation that permits a better accommodation of the severe work-hardening into the material. Nevertheless, the elevation of the pressing force associated to backpressure guarantees the

ISSN 1516-392X

consistency of the proposed model once it represents a physical obstacle to the billet passage towards the die exit channel.

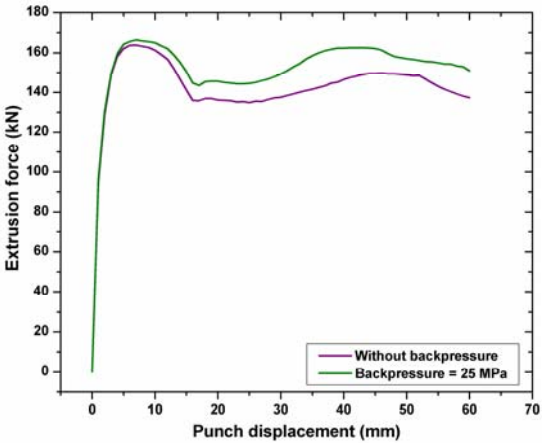

Figure 3. Numerical predictions of extrusion force.

Figure 4 shows the results calculated with the finite element models of effective plastic strain and dislocation density during ECA extrusion of pure cooper. These results were determined for a defined block of finite element and, therefore, represent average predictions. Consistently with the previous discussion about the predictions of processing force, the backpressure caused an stabilization of the effective plastic strain at 1.21 while neglecting this effect the maximum observed value was ~ 1.13 after 31 mm of displacement in both cases, see Figure 4a. At the same time, as the density dislocation is strongly affected by the effective plastic strain in the Kocks-Mecking [19] solution defined in Equation 12, the increasing of the effective plastic strain associated to backpressure provided higher predictions of density dislocations, as presented in Figure 4b.

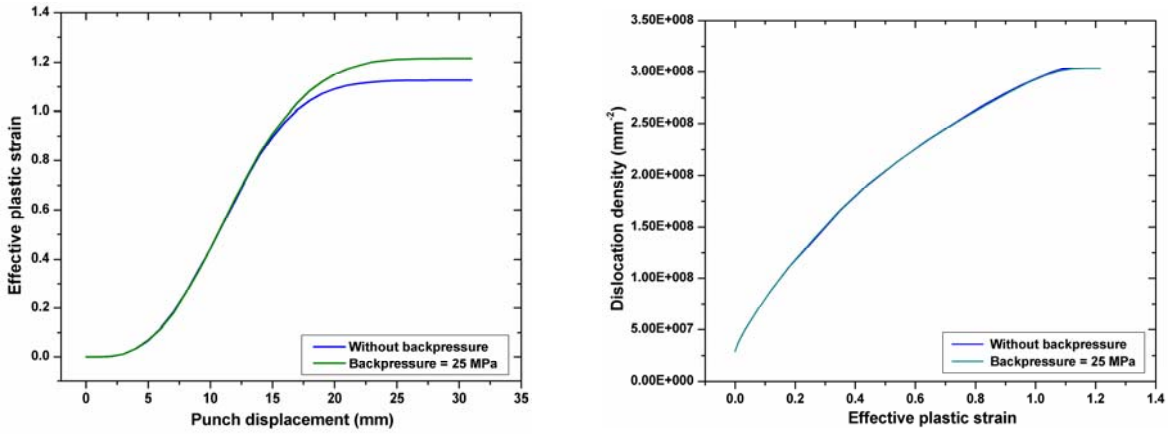

(a) (b)

Figure 4. Finite - element results of: (a) effective plastic strain and (b) dislocation density versus effective plastic strain.

Figure 5 displays the iso-contours of effective plastic strain and density dislocation obtained with the finite element model with backpressure. It is observed a higher uniform zone of effective plastic strain, light green colored in Figure 5a, and the associated distribution of dislocation density along the billet surface that is represented in red (Figure 5b). These deformed geometries are very useful to reinforce the Kocks-Mecking [19] description of the high dependence between

ISSN 1516-392X

dislocation density evolution and the effective plastic strain attributed to material during its severe extrusion process characterized by the ECAE technique.

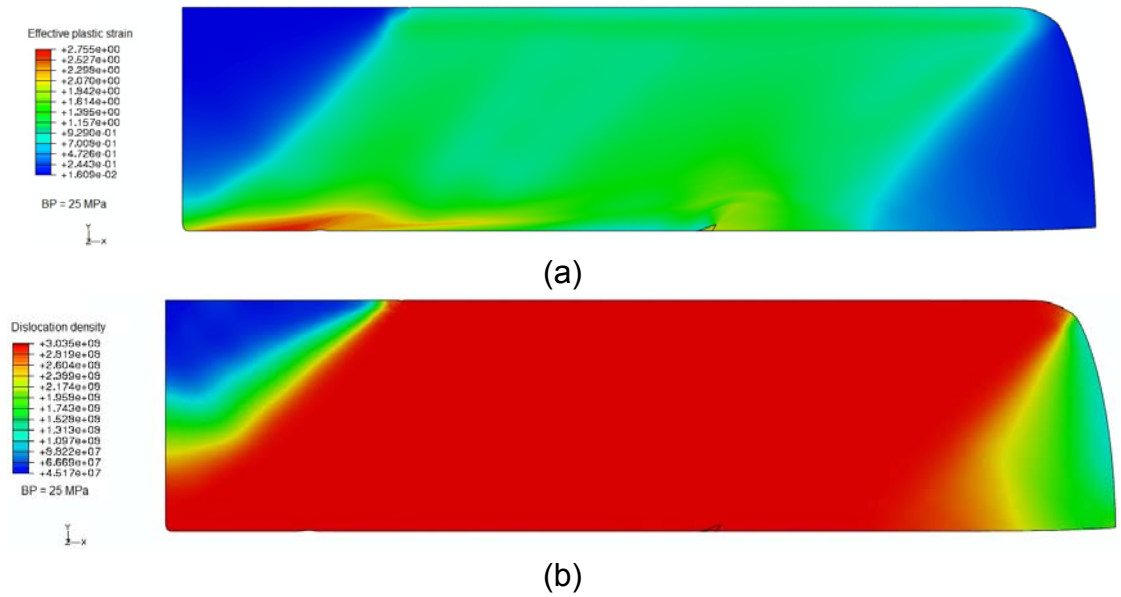

Figure 5. FE iso-contours of: (a) effective plastic strain and (b) dislocation density.

Table 2 lists the analytical and numerical maximum predictions of extrusion force, effective plastic strain and density dislocation for the distinct evaluated conditions in the present work, that is, without backpressure and considering this effect with a magnitude of 25 MPa. Considering the appreciable proximity between the calculated results, it is observed that the proposed analytical model can be validated by the comparing the associated finite element values and it is able to reproduce the materials multiscale plastic behavior during single-pass ECAE processing at room temperature with backpressure effect.

Table 2. Comparison between analytical and numerical results

Performed analyses	Without backpressure		Backpressure = 25 MPa	
	Analytical model	FEM model	Analytical model	FEM model
Extrusion force (kN)	170.50	163.80	180.50	166.00
Effective plastic strain	1.155	1.126	1.155	1.215
Dislocation density (mm^{-2})	$3.03x10^8$	$3.02x10^8$	$3.03x10^8$	$3.03x10^8$

4 CONCLUSIONS

From Kocks – Mecking [19] dislocation-density model, upper-bound solutions and plane strain finite element models were proposed to estimate the extrusion force by including the backpressure effect after single pass processing of pure cooper at room temperature via ECAE technique. Also, the predictions of effective plastic strain and

ISSN 1516-392X

dislocation density evolution were obtained. Based on the present study the following conclusions can be outlined:

- A consistent increasing of extrusion force associated to inclusion of backpressure effect was observed with the finite-element simulations for comparison to the case which this condition was neglected;
- The numerical results of effective plastic strain and density dislocation showed a stabilization at higher values when the backpressure effect was considered in the tooling modeling. It agreed with the behavior observed to extrusion force. Also, the influence of backpressure on the relationship between effective plastic strain and density dislocation evolution could be verified and associated to uniform regions developed along the deformed workpiece surface;
- The proposed analytical model to predict extrusion force, effective plastic strain and density dislocation that includes the backpressure effect could be validated for comparison with the results provided by finite element simulations due to consistency of obtained theoretical predictions.

REFERENCES

1 SEGAL, V.M. Materials processing by simple shear, Materials Science and Engineering A, v. 197, p. 157-164, 1995.
2 IWAHASHI, Y.; WANG, W.; NEMOTO, M.; LANGDON, T.G. Principle of equal-channel angular pressing for the processing of ultra-fine grained materials, Scripta Materialia, v.35, p. 143-146, 1996.
3 SEGAL, V.M. Severe plastic deformation: simple shear versus pure shear, Materials Science and Engineering A, v. 338, p. 331-344, 2002.
4 SEMIATIN, S.L.; SALEM, A.A.; SARAN, M.J. Models for severe plastic deformation by equal-channel angular extrusion, Journal of Materials, v.56, p. 69-77, 2004.
5 SEGAL, V.M. Equal channel angular extrusion: from macromechanics to structure formation, Materials Science and Engineering A, v. 271, p. 322-333, 1999.
6 SEGAL, V.M. Slip line solutions, deformation mode and loading history during equal channel angular extrusion, Materials Science and Engineering A, v. 345, p. 36-46, 2003.
7 ALKORTA, J.; SEVILLANO, J.G. A comparison of FEM and upper-bound type analysis of equal-channel angular pressing (ECAP), Journal of Materials Processing Technology, v. 141, p. 313-318, 2003.
8 PÉREZ, C.J. L. On the correct selection of the channel die in ECAP processes, Scripta Materialia, v. 50, p. 387-393, 2004.
9 GHOLINIA, A.; BATE, P.; PRANGNELL, P.B. Modelling texture development during equal channel angular extrusion of aluminium, Acta Materialia, v. 50, p. 2121-2136, 2002.
10 BEYERLEIN, I.J.; LEBENSOHN, R.A.; TOMÉ C.N. Modeling texture and microstructural evolution in the equal channel angular extrusion process, Materials Science and Engineering A, v. 345, p. 122-138, 2003.
11 TÓTH, L.S.; MASSION, R.A.; GERMAIN, L.; BAIK, S.C.; SUWAS, S. Analysis of texture evolution in equal channel angular extrusion of copper using a new flow field, Acta Materialia, v. 52, p. 1885-1898, 2004.
12 SRINIVASAN R. Computer simulation of the equichannel angular extrusion (ECAE) process, Scripta Materialia, v. 44, p. 91-96, 2001.
13 BAIK, S.C.; ESTRIN, Y.; KIM, H.S.; HELLMIG, R.J. Dislocation density-based behaviour of deformation behaviour of aluminium under equal channel angular pressing, Materials Science and Engineering A, v. 351, p. 86-97, 2003.

ISSN 1516-392X

14 LI, S.; BOURKE, M.A.M.; BEYERLEIN, I.J.; ALEXANDER, D.J.; CLAUSEN, B. Finite element analysis of the plastic deformation zone and working load in equal channel angular extrusion, Materials Science and Engineering A, v. 382, p. 217-236, 2004.
15 NAGASEKHAR, A. V.; TICK-HON, Y. Optimal tool angles for equal channel angular extrusion of strain hardening materials by finite element analysis, Computational Materials Science, v. 30, p. 489-495, 2004.
16 CAZACU, O.; BARLAT, F. Relation of experiments to mathematical theories of plasticity, Mathematics and Mechanics of Solids, v. 6, p. 613-630, 2001.
17 KOCKS, U.F. Laws for work-hardening and Low- Temperature Creep, Journal of Engineering Materials and Technology, Argonne National laboratory, 1976.
18 MECKING, H.; KOCKS, U.F. Kinetics of flow and strain-hardening, Acta Metallurgica, v. 29, p. 1865-1875, 1981.
19 19 DALLA TORRE, F.; LAPOVOK, R.; SANDLIN, J.; THOMSON, P.F.; DAVIES, C.H.J.; PERELOMA, E.V., Microstructures and properties of copper processed by equal channel angular extrusion for 1- 16 passes, Acta Materialia, v.52, p.4819-4832, 2004.
20 KOBAYASHI, S.; OH, S.I.; ALTAN, T. Metal Forming and the Finite-Element Method, Oxford University Press, New York. p. 377, 1989.
21 PÉREZ, C.J.L.; LURI, R. Study of the ECAE process by the upper bound method considering the correct die design, Mechanics of Materials, v. 40, p. 617-628, 2008.
22 MEDEIROS, N.; MOREIRA, L.P.; BRESSAN, J.D.; LINS, J.F.C.; GOUVÊA, J.P. Upper-bound sensitivity analysis of the ECAE process, Materials Science and Engineering A, v.527, p. 2831-2844, 2010.
23 LURI, R.; PÉREZ, C.J.L.; LEÓN, J. A new configuration for equal channel angular extrusion dies, Journal of Manufacturing Science and Engineering, v. 128, p. 860-865, 2006.
24 MOREIRA, L.P.; FERRON, G. Finite element implementation of an orthotropic plasticity model for sheet metal forming simulations. Latin American Journal of Solids and Structures, v. 4, p. 149-176, 2007.
25 MEDEIROS, N.; LINS, J.F.C.; MOREIRA, L.P.; GOUVÊA J.P. The role of the friction during the equal channel angular pressing of an IF-steel billet, Materials Science and Engineering A, v. 489, p. 363-372, 2008.